

0.1 Energy spectra and eigenstates of quasiperiodic tight-binding Hamiltonians

Uwe Grimm

Applied Mathematics Department, Faculty of Mathematics and Computing,
The Open University, Walton Hall, Milton Keynes MK7 6AA, United Kingdom

Michael Schreiber

School of Engineering and Science, International University Bremen,
P.O. Box 750 561, 28725 Bremen, Germany

0.1.1 Introduction

Among the physical properties of quasicrystals [1], their transport properties, such as the electric conductivity, have attracted particular attention. Over the past decades, a lot of experimental and theoretical effort has been spent on the investigation and explanation of transport anomalies in quasicrystals, see [2, 3, 4] for recent collections of review articles and [5] for further references; compare also [6, 7, 8]. Though there undoubtedly exists a strong interrelation between the quasicrystalline structure and the electronic properties [9, 10] — after all, the electrons determine the structure of a solid — it makes sense to consider the properties of electrons in a given aperiodic solid.

The simplest model that may be expected to capture at least some characteristics of electronic properties of quasicrystals is that of a single electron moving in a quasiperiodic background, realised, for instance, by a quasiperiodic potential. Mathematical and theoretical studies of related systems had already been performed prior to the experimental discovery of quasicrystals, see, for instance, the review [11] on the properties of almost periodic Schrödinger operators. In most cases, the models are defined on a discrete space, physically motivated by a tight-binding approach where the electron can hop from one vertex of a graph to any of its neighbouring vertices, and the aperiodicity is introduced either by an aperiodic graph to model the aperiodic solid, or by an aperiodic modulation of the potential or the hopping probabilities.

While quite a lot is known rigorously about one-dimensional systems, see [12] and references therein, higher-dimensional systems, apart from a few particular examples, have mainly been investigated by numerical calculations for finite systems or periodic approximants. Here, we summarise several results for aperiodic tight-binding models in two and three dimensions, which are mainly based on numerical investigations. These concern energy spectra of quasiperiodic tight-binding models and the corresponding energy level statistics, multifractal properties of the eigenstates, and quantum diffusion. In addition, we present some recent results obtained for interacting electrons in one-dimensional systems.

We consider the simplest tight-binding model of a single electron moving on a (quasiperiodic) graph, for instance the graph corresponding to the rhombic Penrose tiling. The Hamiltonian has the form $H_{jk} = t_{jk} + \varepsilon_k \delta_{jk}$, where j and k label the vertices of the graph. In a Dirac bra-and-ket notation with mutually orthogonal states $|j\rangle$ associated to any vertex j , we

have

$$H = \sum_{jk} |j\rangle t_{jk} \langle k| + \sum_k |k\rangle \varepsilon_k \langle k| \quad (1)$$

with matrix elements $H_{jk} = \langle j|H|k\rangle$. Here, t_{jk} play the role of hopping elements between the states associated to vertices j and k , and will usually be considered to vanish except when the two vertices are connected by an edge (bond) of the underlying quasiperiodic graph. In the simplest scenario, the hopping elements are just $t_{jk} = 1$ for vertices connected by an edge and $t_{jk} = 0$ otherwise. The parameters ε_k correspond to on-site energies. As a further simplification, we shall usually choose $\varepsilon_k = 0$ for all vertices k , so no vertex is energetically preferred to any other.

In the simplest case, where the hopping elements t_{jk} are either one or zero and where the on-site energies vanish, the Hamiltonian is just the adjacency matrix of the underlying graph, encoding which vertices are neighbours connected by edges. For an infinite quasiperiodic tiling the matrix will be infinite; in practice, we either consider finite patches and try to extrapolate the results to infinite systems, or investigate a series of periodic approximants, i.e., periodic systems with growing unit cells which approximate the infinite quasiperiodic tiling.

In any case, we are interested in the behaviour of the eigenvalues and the corresponding eigenvectors of these matrices, in particular in the infinite-size limit where the aperiodic system is approached. The eigenvalues and eigenvectors are interpreted as the single-electron energies and the corresponding wave functions. The structure of the density of states (DOS) as a function of the energy, which is defined as the limit of the number of eigenvalues in an energy interval when the size of the interval goes to zero, and the localisation properties of the wave functions are intimately linked to the electronic transport properties.

Quasiperiodic systems are very peculiar in this respect, due to the competition between the aperiodicity on the one hand and the strict quasiperiodic order on the other hand. Aperiodicity means that there is no translation that maps the system into itself, so the system eventually looks different from any of its vertices, even if local configurations may be the same. This variation acts similar to a random disorder and thus favours localisation of wave functions. The quasiperiodic order is reflected in the repetitivity of the tilings, which means that the same local neighbourhoods reappear again and again, albeit not in a periodic fashion. For the examples at hand, this can in fact be phrased more strongly by giving bounds on the distance between appearances of the same patches in the tiling. Repetitivity causes resonances between equivalent local configurations, and thus favours extended wave functions. The result is that wave functions in quasiperiodic tight-binding models are expected to be different from the exponentially localised wave functions found in (strongly) disordered systems, like in the Anderson model of localisation [13], but also different from the Bloch waves found in the periodic situation of a usual crystalline system. Such wave functions are often called ‘‘critical’’, because they appear at the metal-insulator transition in the three-dimensional Anderson model of localisation [14, 15, 16, 17].

The Anderson model of localisation is defined by a single-particle Hamiltonian like (1) on a cubic lattice with a nearest-neighbour hopping term and an on-site energetic disorder. For this simple model, one finds a transition from a metallic phase at small disorder to an insulating phase at large disorder, corresponding to a transition from extended to exponentially

localised eigenstates [18, 19, 20]. At the transition itself, the eigenstates become critical; they are neither extended nor exponentially localised, but show a multifractal distribution of amplitudes [15]. In fact, the expectation that the wave functions in quasiperiodic model systems are neither exponentially localised nor extended Bloch-like states, has been substantiated by rigorous arguments for large classes of one-dimensional discrete aperiodic Schrödinger operators constructed from substitution rules, where it can be shown that their spectrum is purely singular continuous [12], and by numerous numerical investigations of two- and three-dimensional systems.

0.1.2 Energy Spectra and Eigenstates

We start by having a look at the spectrum of tight-binding Hamiltonians of this kind. Typical results for the DOS and the integrated density of states (IDOS), which just counts the number of eigenvalues up to a given energy E , are shown in Fig. 1 for examples in one, two and three spatial dimensions.

In the one-dimensional case, the example used is the co-called octonacci chain [21]. In one dimension, choosing all hopping parameters as one and all on-site energies as zero yields

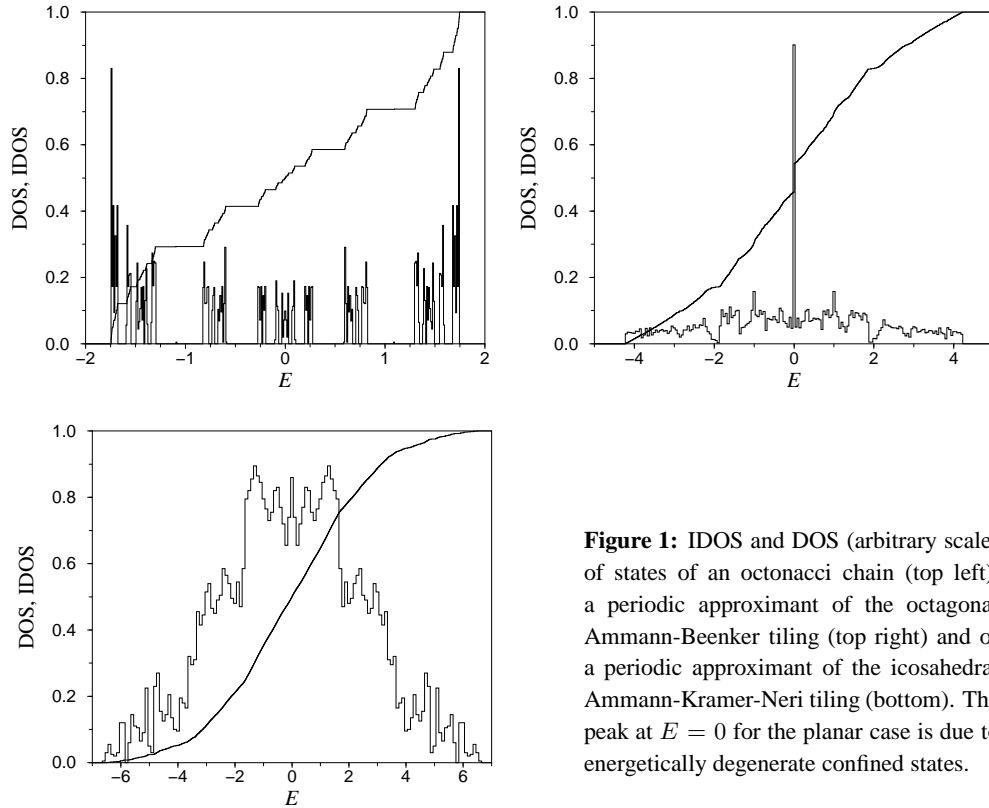


Figure 1: IDOS and DOS (arbitrary scale) of states of an octonacci chain (top left), a periodic approximant of the octagonal Ammann-Beenker tiling (top right) and of a periodic approximant of the icosahedral Ammann-Kramer-Neri tiling (bottom). The peak at $E = 0$ for the planar case is due to energetically degenerate confined states.

the simple periodic chain, so we have to introduce some parameter in order to have a non-trivial aperiodic system. In this case, this is conveniently achieved by assigning two values $t_{j,j+1} \in \{1, v\}$ for the hopping parameters such that the sequence of hopping parameters along the chain is aperiodic; choosing an aperiodic sequence for the on-site energies would lead to very similar results. For the octonacci chain, the sequence is obtained from the two-letter substitution rule

$$\varrho: \begin{array}{l} S \rightarrow L \\ L \rightarrow LSL \end{array} \quad (2)$$

applied repeatedly on the initial word $w_0 = S$, so $w_m = \varrho^m(w_0)$. The limit word is semi-infinite aperiodic sequence $w_\infty = LSLLLSLLSLLSLLLSL\dots$. We now choose the hopping parameters as $t_{j,j+1} = 1$ if the j th letter in w_∞ is an L , and as $t_{j,j+1} = v$ if it is an S . The spectrum shown in Fig. 1 corresponds to a parameter value $v = 1/2$.

For such systems, it is known that the spectrum is purely singular continuous, and is a Cantor set of zero Lebesgue measure [12]. This is reflected in the apparent set of gaps in the spectrum; the possible positions of the corresponding plateaux in the IDOS are also known by Bellissard's gap labelling theorem [22]. One powerful method to tackle one-dimensional system employs the so-called trace maps, see [23, 24] and references therein for details.

The two-dimensional example in Fig. 1 corresponds to a periodic approximant of the octagonal Ammann-Beenker tiling [25, 26, 27, 28]; in this case all hopping parameters are chosen as one along the edges and zero otherwise. The same choice applies to the three-dimensional system, which corresponds to a periodic approximant of the icosahedral Ammann-Kramer-Neri tiling [29]. There is a clear tendency of smoothing of the spectrum as the dimension increases, and there are only a few, if any, gaps in the spectrum. One particularity of the two-dimensional case is the pronounced peak in the centre of the spectrum at energy $E = 0$, which is due to families of strictly localised or ‘‘confined’’ states supported on a finite number of vertices, which, due to the repetitivity of the tiling, reappear at various places throughout the tiling and make up a finite fraction of all states, see [30] and references therein. This is a consequence of the local topology of the tiling, and also happens for the tight-binding model on a rhombic Penrose tiling [30].

Some properties of such energy spectra will be discussed below in more detail, including the level-spacing distribution and fractal dimensions of the spectral measure. But first we are going to discuss some general features of the eigenstates that are observed numerically for two and three-dimensional tight-binding Hamiltonians defined on quasiperiodic tilings.

Again, the one-dimensional situation has been studied in much detail, see [12] and references therein for details. For many models based on substitution sequences, such as our example of the octonacci chain, it is known rigorously that the generalised eigenstates are neither exponentially localised — in which case they would correspond to proper eigenvalues and hence yield a discrete spectrum — nor extended over the entire system. These are the critical states mentioned previously. However, this is definitely not true for all one-dimensional aperiodic discrete Schrödinger operators; a classical example is provided by the Aubry-André or Harper model, in the mathematical literature also known as the almost-Mathieu equation, see [31, 32] and references therein. This model is also a one-dimensional quasiperiodic tight-binding model, but now the local on-site potential takes values in a continuous interval, in contrast to the substitution models discussed above. The potential at position j of the chain,

where j is an integer, has the form $V(j) = 2\mu \cos(\alpha j + \beta)$, which is aperiodic provided $\alpha/2\pi$ is irrational. This model behaves rather differently from the substitution chains, and details may even depend on the type of irrationality of $\alpha/2\pi$ — irrational numbers that are too well approximated by rational numbers may show a non-generic behaviour. In most cases, the golden mean or its inverse is used [31]. Depending on the strength of the quasiperiodic potential, one finds, for $\mu < 1$, a metallic phase where *all* eigenstates are extended, and the spectrum is absolutely continuous, and, for $\mu > 1$, an insulating phase, where *all* eigenstates are exponentially localised, and the spectrum is pure point. Here, the hopping parameter was assumed to be unity. For the critical value $\mu = \mu_c = 1$, one observes a metal-insulator transition with multifractal eigenstates, similar to that found in the three-dimensional Anderson model of localisation [13, 15, 16, 17] and also similar to the behaviour of substitution-based systems like the octonacci chain. In contrast to the Anderson model, there are no mobility edges [17] in the Aubry-André model — at the value $\mu_c = 1$ the entire spectrum localises. And, of course, there is no randomness whatsoever in this model — the metal-insulator transition takes place solely as a consequence of the quasiperiodic potential strength. This model has also been used as a one-dimensional toy model to study the effects of an electron-electron interaction on the metal-insulator transition [32, 33, 34, 35, 36], see Sec. 0.1.6 below.

In general, it is expected that generalised eigenstates of tight-binding Hamiltonians on aperiodic tilings of the plane, and probably also in three dimensions, are also critical, i.e., neither exponentially localised nor extended. However, no mathematically rigorous results exist as yet, so conclusions are based on numerical observations. A simple quantity that characterises the degree of localisation of a generalised eigenstate with amplitudes ψ_j at vertex j is the participation number P defined by

$$P^{-1} = \sum_{j=1}^N |\psi_j|^4, \quad (3)$$

where N denotes the total number of vertices in our finite approximant. The participation number tells us how many vertices carry a significant part of the probability measure given by $|\psi_j|^2$. The ratio $p = P/N$, the participation ratio, thus contains a crude information about

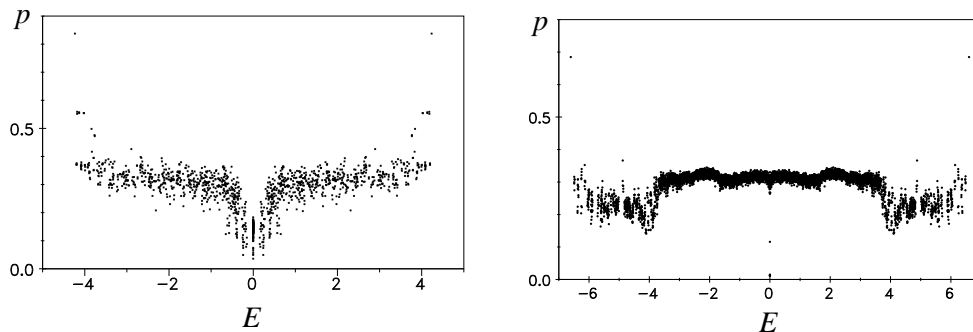


Figure 2: Participation ratios $p = P/N$ for eigenstates of periodic approximants of the rhombic Penrose tiling (top) and the Ammann-Kramer-Neri tiling (bottom).

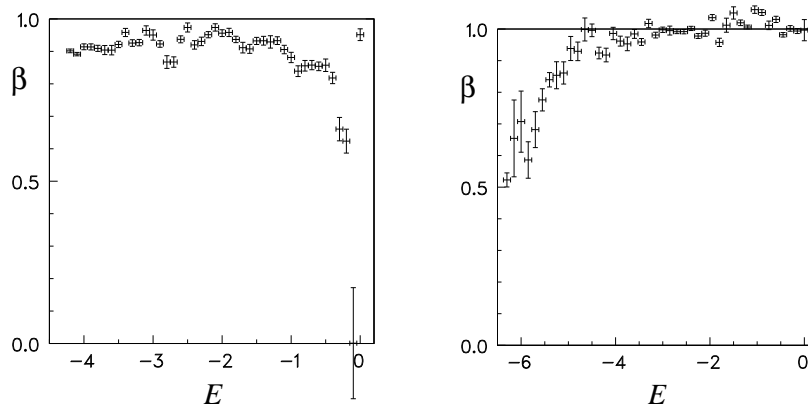


Figure 3: Estimated scaling exponents β of the participation number for eigenstates of the Penrose tiling (left) and of the Ammann-Kramer-Neri tiling (right).

the degree of localisation of the wave packet described by the state ψ_j . Numerical results for large periodic approximants of the Penrose and the Ammann-Kramer-Neri tiling are shown in Fig. 2. They indicate that, for the system size under consideration, the participation ratio lies around 0.3, and there appears to be a tendency towards a stronger localisation in the “band” centre for the Penrose tiling, while in the icosahedral case states near the “band” edges appear to be more localised.

However, what we actually need to know in order to obtain information about localisation properties in the infinite tiling is the scaling behaviour of the participation number with the size of the approximant. For an extended state, we expect P to grow linearly with N , whereas for a localised state P will eventually be constant. For our critical states, which sometimes are also referred to as algebraically localised states, we expect a scaling behaviour $P \sim N^\beta$ with some exponent $0 \leq \beta \leq 1$. Note that $\beta = 0$ for exponentially localised states, and $\beta = 1$ for extended states; so any value $0 < \beta < 1$ points towards the presence of critical states. The converse is not true — if $\beta = 0$ or $\beta = 1$ we cannot immediately deduce that the state is exponentially localised or extended, respectively, as we only consider one moment of the distribution; for instance, a sufficiently rapid sub-exponential decay may still give $\beta = 0$. Numerical results, again for the Penrose and the Ammann-Kramer-Neri tiling, are displayed in Fig. 3. The values of the exponent β for the Penrose tiling are about 0.9, clearly below one, for most energies except near the centre of the “band” where they are smaller. This is consistent with a preponderance of multifractal eigenstates which are neither extended nor exponentially localised. In the three-dimensional case, the result is less obvious. Whereas states near the “band” edge clearly show $\beta < 1$, the majority of states yields values for the exponent β which are consistent with extended states. In these cases, it may be that the system size is simply insufficient to resolve values of β close to, but smaller than one. However, we also cannot exclude the possibility that $\beta = 1$ for a large part of the spectrum. Still, as mentioned previously, this does not automatically imply that the eigenstates are extended.

Another, more powerful approach to characterise “critical” states is given by a multifractal

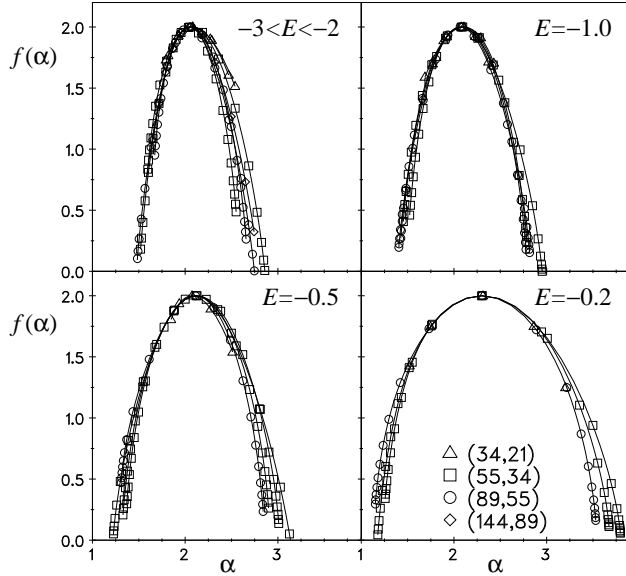


Figure 4: Singularity spectra $f(\alpha)$ for various eigenstates of periodic approximants of the Penrose tiling. The approximants are labelled by two integers whose ratio is a rational approximation of the golden mean $\tau = (1 + \sqrt{5})/2$.

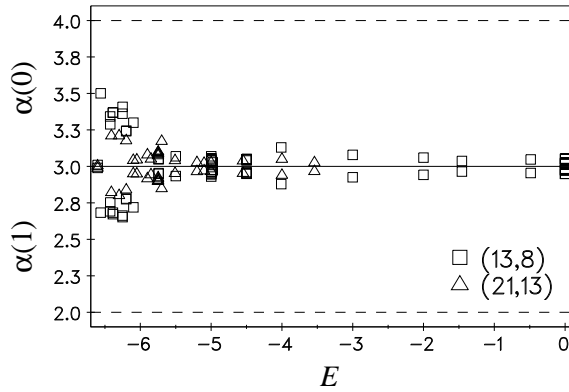


Figure 5: Singularity strengths $\alpha(0)$ and $\alpha(1)$ for eigenstates of the Ammann-Kramer-Neri tiling. The approximants are labelled by two integers whose ratio is a rational approximation of τ .

analysis. In the standard box-counting approach, the system is divided into boxes of linear size δ . We consider the measures of the normalised q th moment $\mu_k(q, \delta)$ of the probability amplitudes $\mu_k(\delta)$ in the boxes labelled by k . We obtain the Lipschitz-Hölder exponent or singularity strength α of an eigenstate and the corresponding fractal dimension f by

$$\alpha(q) = \lim_{\delta \rightarrow 0} \sum_k \frac{\mu_k(q, \delta) \ln \mu_k(1, \delta)}{\ln \delta}, \quad f(q) = \lim_{\delta \rightarrow 0} \sum_k \frac{\mu_k(q, \delta) \ln \mu_k(q, \delta)}{\ln \delta}, \quad (4)$$

yielding the characteristic singularity spectrum $f(\alpha)$ in a parametric representation. According to [17], the generalized fractal dimensions D_q^ψ can be obtained via a Legendre transformation $D_q^\psi = \{f[\alpha(q)] - q\alpha(q)\}/(1 - q)$.

Some results for the Penrose and Ammann-Kramer-Neri tiling are shown in Figs. 4 and

5, respectively [37]. Clearly, eigenstates on the Penrose tiling show characteristic multifractal behaviour, with singularity spectra $f(\alpha)$ that are nearly independent of the system size. Towards the “band” centre, the singularity spectra become wider, indicating a larger degree of localisation. On the basis of our numerical analysis, we cannot draw similar conclusions for the icosahedral case, as the singularity strengths $\alpha(0) = D_0^\psi$ and $\alpha(1) = D_1^\psi$ shown in Fig. 5 are very close to 3, the value for extended states, except near the “band” edges.

Summarising the results mentioned so far, we have the situation that the characterisation of spectra and eigenstates is rather advanced for one-dimensional aperiodic Schrödinger operators, with a number of mathematically rigorous results available. For planar quasiperiodic tilings, numerical results strongly favour the conjecture that typical eigenstates are neither extended nor exponentially localised, but have multifractal characteristics. In the three-dimensional case, the situation is less clear. One might expect a rather similar behaviour as in two dimensions, but numerical results are inconclusive. They do not rule out that large parts of the spectrum might contain extended states, although the behaviour of the so-called structural entropy considered in [38] hints at a power-law decay. However, introducing a random energetic disorder (like in the Anderson model) in the icosahedral tight-binding model leads to a localisation transition which appears to be very similar to the metal-insulator transition observed in a simple cubic lattice [39], which might be regarded as evidence favouring the existence of extended states. The main problem with all these results is that they may simply be artifacts of the finite system size which might yet be too small to resolve the multifractal behaviour.

0.1.3 Level-Spacing Distribution

We now return to discuss a rather different property of the energy spectrum, the statistics of the energy level distribution. The statistical analysis of energy levels was originally applied to the complex energy spectra of nuclei, but has since been shown to be relevant to many complex systems. In the Anderson model of localisation, the localisation transition is accompanied by a qualitative change in the normalised distribution $P_0(s)$ of spacings between adjacent energy levels [18, 19, 40]. For the weakly disordered, metallic phase, the level-spacing distribution $P_0(s)$ is well described by the corresponding distribution $P_0^{\text{GOE}}(s)$ of the Gaussian orthogonal ensemble of random matrix theory [41], reflecting the level repulsion or hybridisation of neighbouring extended states. In the strongly disordered regime, where eigenstates are exponentially localised, the spacing is described by a Poisson law $P_0^{\text{P}}(s) = \exp(-s)$, because the localised states can be arbitrarily close in energy. These results are universal in the sense that they do not depend on details of the model, but are a general feature of a large class of systems sharing a few general properties.

At the metal-insulator transition, the level-spacing distribution has been shown to follow yet another behaviour which is attributed to the existence of a “critical ensemble” [42]. In contrast to the other two cases, this “critical” level-spacing distribution appears to be non-universal. A sketch of the three level-spacing distributions is given in Fig. 6, where the critical curve corresponds to the function discussed in [42].

As discussed above, eigenstates in planar quasiperiodic tight-binding models appear to be generically multifractal, and thus similar to the eigenstates found at the metal-insulator transition of the Anderson model of localisation. In the latter model it is extremely difficult to

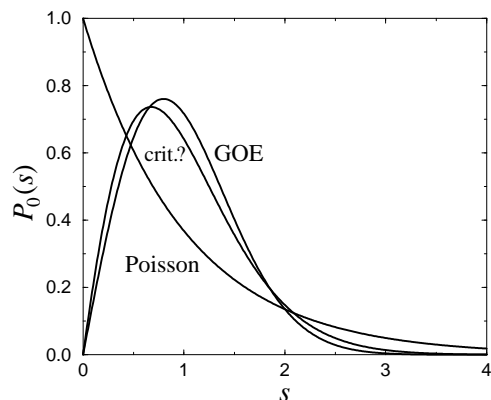


Figure 6: The level-spacing distribution $P_0^{\text{GOE}}(s)$ of the Gaussian orthogonal ensemble of random matrix theory, the Poisson law $P_0^{\text{P}}(s) = \exp(-s)$ and a suggested “critical” distribution [42].

do level-spacing analysis at criticality, because only states near the mobility edge may be taken into account. In planar quasiperiodic tight-binding models, however, we have a large reservoir of multifractal states, and thus we might expect to find some “critical” statistics intermediate between the Poisson behaviour and the universal random matrix distribution.

Indeed, early investigations found significant deviations from the random matrix behaviour [43,44]. However, the system considered in these papers is a standard periodic approximant of the Ammann-Beenker tiling [25, 26, 27, 28] which is a singular patch with an exact reflection symmetry along a diagonal, but with the property that the fourfold rotational symmetry is broken only “weakly”. In Fig. 7, such an approximant is shown, overlaid with a copy rotated by 90 degrees. This shows that mismatches occur only along “worms”. Although this is no exact symmetry, and hence the energy spectrum does not split into independent sectors, it may influence the level-spacing distribution and thus lead to non-generic results [45].

A careful re-investigation of the energy spectrum for the tight-binding Hamiltonian on the Ammann-Beenker tiling, where the on-site energies are chosen to be zero and hopping elements are one along the edges of the tiling, shows that for generic patches the level-spacing distribution is in fact very well described by the random matrix distribution [45, 46, 47, 48]. In Fig. 8, the numerical results obtained by diagonalising the tight-binding Hamiltonian for an eightfold symmetric patch of the Ammann-Beenker tiling with 157 369 vertices are shown. In this case, we need to consider a single irreducible sector corresponding to one of the ten irreducible representations of the exact D_8 symmetry of the patch. Here, we not only considered the normalised spacing distributions $P_0(s)$, in terms of the mean level spacing s , for adjacent energy levels, but also the corresponding spacing distributions $P_n(s)$ of pairs of energy levels such that the energy interval between the two states contains n further levels. The numerical results for $n = 0, 1, 2, 3$ are shown in Fig. 8 and compared with the universal spacing distributions $P_n^{\text{GOE}}(s)$ of the Gaussian orthogonal random matrix ensemble [41, 48]. The agreement is extremely good, considering the finite size of the patch. This was already noticed in [46] where it was shown that the exact random matrix distribution $P_0^{\text{GOE}}(s)$ fits the numerical distribution better than Wigner’s surmise $P_0^{\text{W}}(s) = \pi s \exp(-\pi s^2/4)/2$, which is a good approximation of $P_0^{\text{GOE}}(s)$. This result has also been verified for different patches and boundary conditions [45, 46, 47, 48], and other planar quasiperiodic systems [49]. Similar

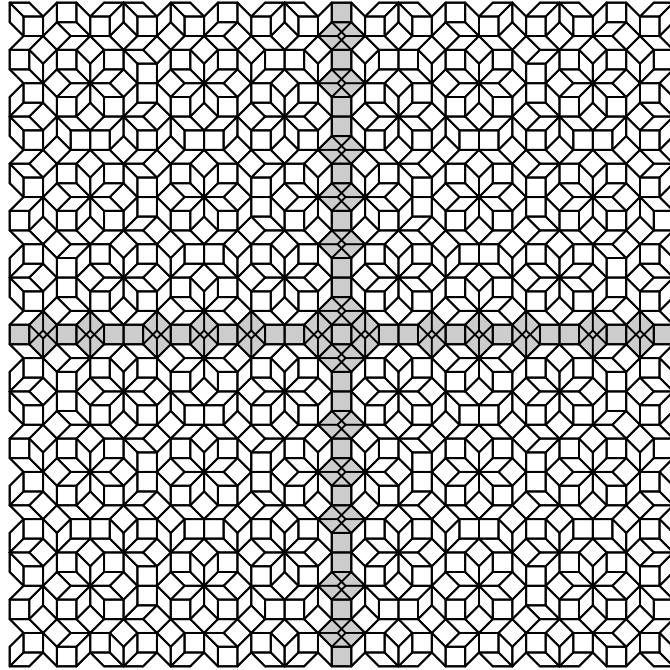


Figure 7: Unit cell of a periodic approximant of the Ammann-Beenker tiling, overlaid by a copy of itself rotated by 90 degrees. Mismatches only occur in the grey shaded “worms” [28].

results were also found in topologically disordered systems [50].

There is, however, a non-trivial step involved in extracting the spacing distributions shown in Fig. 8 from the raw eigenenergies of the finite system. As Fig. 1 shows, the DOS varies considerably over the spectrum, and we have to correct for this variation if we wish to compare with the universal random matrix distributions. This process, known as “unfolding”, is rather tricky in our case because it requires a clear distinction between different scales. On the one hand, we need to average out the fluctuations in the DOS, so we average on a scale that is given by the fluctuations, see Fig. 1. On the other hand, we are looking at the spacing distribution of energy levels, so averaging has to be done on a scale that is large compared to the mean level spacing. It is not easy to fulfill these two requirements for planar quasiperiodic tight-binding models, because the two scales do not seem to be well separated, at least for relatively small systems, compare also [51] for an approach based on the inflation symmetry of the tiling. Here, we used a simple unfolding procedure by approximating the IDOS by a smooth spline function [45, 46, 47, 48].

There is one direct way to check that the unfolding procedure does not introduce artifacts in our results [47]. If we consider the level-spacing distribution for levels within small energy intervals such that the DOS is approximately constant on the interval, we do not need to apply any unfolding procedure and can compare the result directly with the universal distribution function. However, the price we pay is that the statistics are much worse, as only the

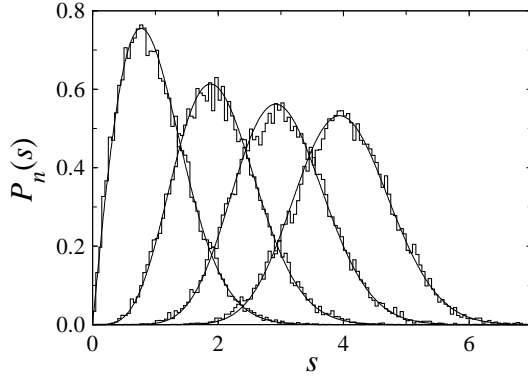


Figure 8: The histograms show the level-spacing distributions $P_n(s)$, $n = 0, 1, 2, 3$ (from left to right), as obtained from the unfolded numerical spectrum of the tight-binding Hamiltonian on an eightfold symmetric patch of the Ammann-Beenker tiling containing $N = 157\,369$ vertices. The smooth curves are the corresponding level-spacing distributions $P_n^{\text{GOE}}(s)$.

limited number of eigenenergies in the chosen interval contributes. Fig. 9 shows the result for three energy intervals. The numerical results for the integrated level-spacing distribution $I_0(s) = \int_s^\infty P_0(t) dt$, with and without unfolding, are compared with the log-normal distribution favoured in [43, 44] and with the integrated level-spacing distribution $I_0^{\text{GOE}}(s)$ of the Gaussian orthogonal random matrix ensemble.

Comparing the energy intervals considered in Fig. 9 with the DOS displayed in Fig. 1, it is apparent that spacing distributions for an approximately constant DOS (for instance, for $3.2 \leq E \leq 3.3$) exhibit random matrix behaviour even without unfolding. However, for energy ranges with fluctuating DOS, the integrated level-spacing distribution $I_0(s)$, without unfolding, deviates from $I_0^{\text{GOE}}(s)$. In the interval $0.5 \leq E \leq 1.5$ with large fluctuations, the level-spacing distribution of the raw eigenenergies is neither well described by a log-normal distribution nor by $I_0^{\text{GOE}}(s)$. For the entire spectrum, the distribution of the raw spacings is actually close to a log-normal distribution, but it is our interpretation that this is due to the abundance of large spacings due to the fluctuations in the DOS. Clearly, the unfolded distribution functions for the three energy intervals agree well with each other and with the spacing distribution of the Gaussian random matrix ensemble.

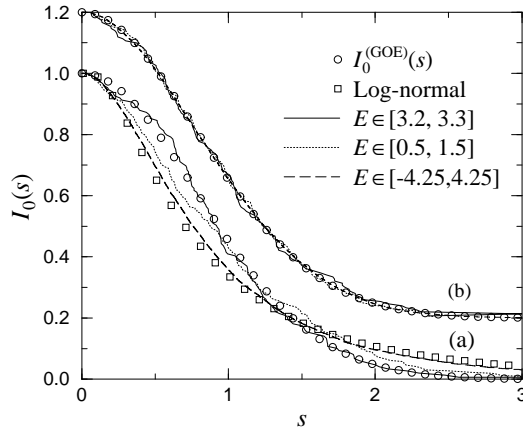


Figure 9: Integrated level-spacing distribution $I_0(s)$ obtained (a) without unfolding and (b) with unfolding for various parts of the spectrum of one sector of the same D_8 -symmetric patch as in Fig. 8: whole spectrum (dashed line), $0.5 \leq E \leq 1.5$ (dotted line), and $3.2 \leq E \leq 3.3$ (solid line). Circles and boxes denote $I_0^{\text{GOE}}(s)$ and the log-normal distribution, respectively. The curve for $I_0(s)$ in (b) has been shifted by 0.2 for clarity.

In conclusion, the spectra of planar quasiperiodic tight-binding models of the type considered here appear to obey random matrix statistics. Compared to the results for the Anderson model, this means that, at least in this respect, they behave like weakly disordered systems rather than like systems at a metal-insulator transition, in spite of their multifractal eigenstates.

0.1.4 Multifractal Eigenstates on the Penrose Tiling

We now come back to the eigenstates of planar quasiperiodic tight-binding models. As mentioned above, numerical results indicate that typical states of hopping models on planar quasiperiodic tilings are multifractal, with certainly some exceptions such as single extended states at the “band” edges and confined states in the “band” centre. For the rhombic Penrose tiling, the confined states can be explicitly constructed, see [30] and references therein, and they make up a sizeable fraction of the spectrum. This is also the case for the Ammann-Beenker tiling as can be seen from the pronounced peak in the “band” centre in Fig. 1.

However, it is also possible to construct some multifractal eigenstates on the Penrose tiling explicitly. This can be achieved by following an ingenious idea of Sutherland [52] to exploit the matching rules of the tiling to derive a non-trivial ansatz for a multifractal wave function. Based on this idea, non-normalisable eigenstates of the centre model, where electrons may hop between neighbouring tiles rather than neighbouring vertices, were derived, and their multifractal properties were characterised [53].

Here, we apply the same idea to the vertex model on the Penrose tiling, i.e., electrons may hop from one vertex of the Penrose tiling to its neighbouring vertices. It turns out that we have to generalise our model slightly in order to find non-trivial solutions [54]. Therefore, we include hopping along the diagonals of the rhombic tiles, with hopping parameters in the Hamiltonian (1) chosen as $t_{jk} = 1$ between two vertices j and k connected by an edge of the tiling, $t_{jk} = d_1, d_2, d_3, d_4$ between vertices j and k on the four different diagonals of the two rhombs, see Fig. 10, and $t_{jk} = 0$ otherwise, and on-site energies $\varepsilon_k = 0$.

As mentioned, the ansatz for the eigenstates of our Hamiltonian on the infinite tiling involves the matching rules of the Penrose tiling. These are usually encoded in a decoration of the tiling with two types of arrows, single and double arrows, located on the edges of the tiles, see Fig. 11 for an example. The matching rules require that two tiles can only share an edge if the corresponding arrow decorations match, both in type and direction. Given such a decoration of the infinite tiling, we define a “potential” or “height function” as follows. First, we choose an arbitrary vertex k_0 on the tiling and define the height of this vertex as $m(k_0) = 0$. Then, for any vertex k , we consider any path consisting of a sequence of edges that connects k_0 to k . The height $m(k)$ is given by counting the number of double arrows encountered along the path, where double arrows pointing along the direction from k_0 to k count as 1, whereas

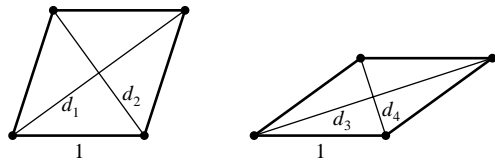


Figure 10: The hopping elements for our tight-binding model on the Penrose tiling are chosen as $t_{jk} = 1$ along the edges of the tiling, and as $t_{jk} = d_1, d_2, d_3, d_4$ along the four different diagonals of tiles.

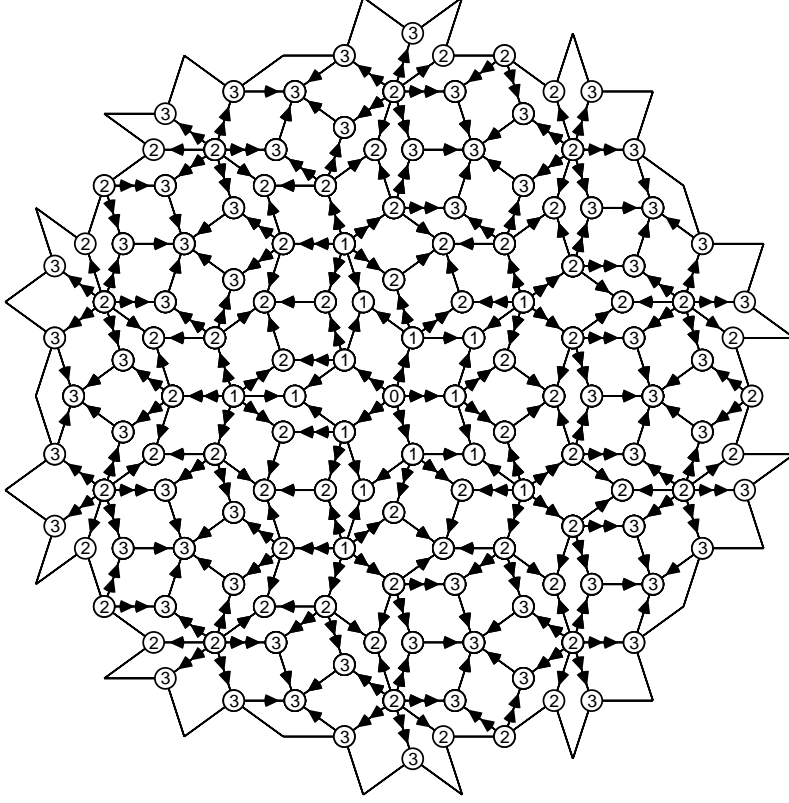


Figure 11: Arrow decoration for vertices k on a patch of the rhombic Penrose tiling encoding the matching rules and the values of the height function $m(k)$ with respect to the centre vertex.

arrows counting in the opposite direction count as -1 . This is well defined because for any closed path this number is zero, as can easily be verified for the two basic tiles. The height at any vertex is thus an integer number. Its actual value depends on our choice of k_0 , but any other choice k'_0 , defines a height function m' that differs from the potential or height function m defined by k_0 only by a constant $m(k'_0)$. Note that the word “potential” is used in a different context here, there are no on-site potentials in our Hamiltonian. The height function $m(k)$ is going to appear in the ansatz for the eigenfunction.

For the Hamiltonian on the infinite tilings, we need to solve the infinite set of equations

$$\sum_k t_{jk} \psi_k = E\psi_j, \quad (5)$$

where $t_{jk} = t_{kj} \in \{0, 1, d_1, d_2, d_3, d_4\}$ as described above. Our ansatz for the amplitudes ψ_j of the wave function at vertex j involves the height function $m(j)$ and information about the

local neighbourhood of the vertex j [54]. In the simplest case, we choose

$$\psi_j = A_{\nu(j)} \gamma^{m(j)}, \quad (6)$$

where $A_{\nu(j)}$ are eight constants corresponding to the eight different vertex stars $\nu(j)$ in the decorated Penrose tiling, and γ is another parameter. Altogether we have nine free parameters in the ansatz, as well as the four hopping parameters d_1, d_2, d_3, d_4 and the energy E . Inserting the ansatz (6) into our infinite set (5) of equations reduces the number of independent equations for our parameters to a finite number, namely 31 equations. Essentially, the equations can be labelled by the different vertex types in the Penrose tiling taking into account the next-nearest neighbours, as for each such patch around a vertex j all vertex types and values of the height function for the vertices k that enter Eqs. (5) are determined.

Even though the number of equations is still more than twice as large as the number of parameters, there exist indeed solutions [54]. It turns out that two different amplitudes $A_{\nu(j)}$ suffice in the ansatz (6), and the wave functions for our solutions do not depend on the vertex type $\nu(j)$, but only on the translation class $t(j)$. The vertices of the Penrose tiling fall into four such translation classes, corresponding to the four disjoint parts of the window in the description as a four-component model set [3, 4, 55]. It follows from Eqs. (5) that the coefficients $A_{\nu(j)}$ have to coincide for vertices of translation classes $t(j) \in \{1, 4\}$, which correspond to the small pentagon as a window, and for vertices of translation classes $t(j) \in \{2, 3\}$, which correspond to the large pentagon as a window.

There are three sets of parameters that solve the eigenvalue equations of (5). It is convenient to introduce the notation $c_{\pm} = 1/(\gamma \pm \gamma^{-1})$ as this combination appears repeatedly in the expressions for the parameters. Explicitly, the three solutions look as follows.

The first solution has the form

$$\psi_j^{(1)} = \begin{cases} (1 - 2\gamma^2)\gamma^{m(j)} & \text{for } t(j) \in \{1, 4\} \\ \gamma^{m(j)+1} & \text{for } t(j) \in \{2, 3\} \end{cases} \quad (7)$$

with hopping parameters $d_1 = c_-/2, d_2 = -3c_-/4 + c_-^{-1}, d_3 = -c_-/4 + c_-^{-1}/2, d_4 = c_-$, and an energy eigenvalue $E = -5c_-/2$. The other two solutions are given by

$$\psi_j^{(2)} = \begin{cases} \gamma^{m(j)} & t(j) \in \{1, 4\} \\ \gamma^{m(j)+1} & t(j) \in \{2, 3\} \end{cases}, \quad \psi_j^{(3)} = \begin{cases} \gamma^{m(j)+1} & t(j) \in \{1, 4\} \\ \gamma^{m(j)} & t(j) \in \{2, 3\} \end{cases}, \quad (8)$$

with $d_1 = -c_+, d_2 = 3c_+/2 - c_+^{-1}/2, d_3 = -(1 + 2\gamma^2)c_+/2, d_4 = (1 - \gamma^{-2})c_+$, and eigenvalue $E = 5c_+$ for the solution $\psi_j^{(2)}$, and with $d_1 = -(1 + 2\gamma^2)c_+/2, d_2 = c_+/4 - c_+^{-1}/2, d_3 = -(1 + 4\gamma^{-2})c_+/4, d_4 = -c_+$, and eigenvalue $E = 5c_+/2$ for $\psi_j^{(3)}$, respectively.

These three solutions contain one free parameter, namely γ . For any value of γ , Eqs. (7) and (8) give solutions of the eigenvalue equations of (5). Note that not only the hopping parameters d_1, d_2, d_3 and d_4 are fixed by γ , but also the eigenvalue E is determined. In other words, this means that for a given Hamiltonian, i.e., for a given set of hopping parameters, our solutions will give at most one eigenfunction, so we cannot gain any global information on the spectrum from this result.

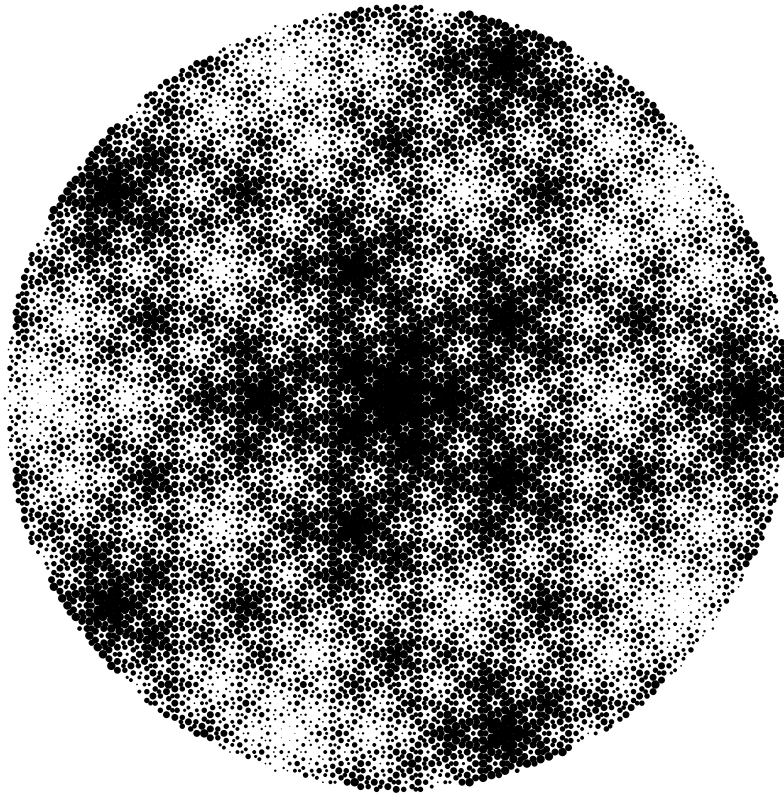


Figure 12: Sketch of the wave function (7) with $\gamma = 3/5$. The probability density $|\psi_j|^2$, encoded in dots of different sizes, is shown on a finite patch of $N = 16\,757$ vertices.

An example wave function is shown in Fig. 12. Clearly, the probability distribution $|\psi_j|^2$ reflects the topology of the tiling, because it essentially depends on the height function $m(j)$ only. The wave functions constructed in this way are not normalisable; for generic values of γ they are neither exponentially localised nor extended. As expected for the generic wave functions, they are multifractal. Generalised dimensions characterising the eigenstates can be calculated by using the inflation symmetry of the tiling and investigating the behaviour of the height function under inflation [54]. The results for the generalised dimensions D_q for various values of γ are shown in Fig. 13. The smaller the value of $|\gamma|$, the faster the wave function decays, giving rise to steeper curves for D_q as a function of q . For $\gamma = 1$, the amplitudes ψ_j are independent of the height function $m(j)$, the wave function is extended, and $D_q = 2$ is constant.

We note that the ansatz (6) can be generalised by taking into account larger coroneae of the vertex j . This has been investigated in [54], and it was shown that the eigenvalues E for the functions constructed here are always infinitely degenerate. However, numerical investigations indicate that, contrary to the case of the confined states [30], these states do not make

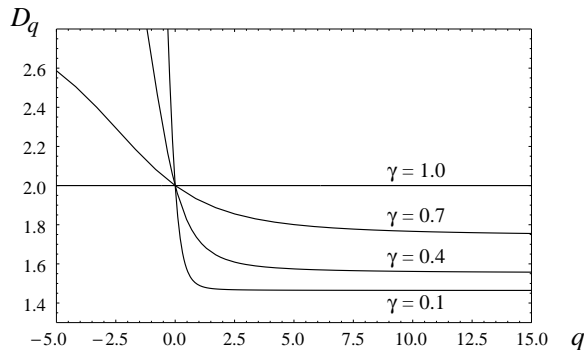


Figure 13: Generalised dimensions D_q for the eigenfunction (7) constructed by the ansatz (6), for various values of γ .

up a finite fraction of the complete spectrum, so they do not lead to a peak in the DOS.

In summary, we can construct particular eigenstates for the infinite Penrose tiling explicitly, following an idea by Sutherland [52]. This at least shows that multifractal states exist in the spectra of such tight-binding Hamiltonians, corroborating the expectation that these states are generic in planar quasiperiodic tight-binding models. However, the price to pay is that we only obtain eigenstates at a particular energy, and thus do not gain any information about the spectrum. The way in which the matching rules are used to construct eigenfunctions of a discrete Schrödinger operator is very interesting; it appears plausible that the height function admits further interpretations as a characteristic feature of the Penrose tiling.

0.1.5 Quantum Diffusion on the Labyrinth

After characterising the spectrum and the eigenstates, we are now interested in the quantum diffusion in quasiperiodic systems. Clearly, the diffusion properties of quasicrystals are associated with the complex eigenstates and energy spectra discussed above [56]. In what follows, we consider two quantities characterising the spreading of wave packets [57], the temporal autocorrelation function $C(t)$ and the mean square displacement $d(t)$. These are defined by

$$C(t) = \frac{1}{t} \int_0^t |\psi_{j_0}(t')|^2 dt', \quad d^2(t) = \sum_j |\mathbf{r}_j - \mathbf{r}_{j_0}|^2 |\psi_j(t)|^2, \quad (9)$$

where $\psi_j(t)$ is the amplitude of the wavefunction at time t at vertex j , which is located at the position \mathbf{r}_j in space. The function $C(t)$ is the time-averaged probability of a wave packet staying at the initial site j_0 at time t , whereas $d(t)$ determines the spreading of a wave packet.

Generally, these two functions are characterised by asymptotic power laws $C(t) \sim t^{-\delta}$, $d(t) \sim t^\beta$ for large time t , where $0 < \delta < 1$ and $0 < \beta < 1$ for one-dimensional quasiperiodic systems [56, 57]. An intimate relation between the spectral properties, in particular the fractal dimensions of the spectrum and the eigenstates, and the exponents δ and β characterising anomalous diffusion is expected on general grounds [58, 59], and is reasonably well established for one-dimensional systems. However, only few two-dimensional quasiperiodic systems have been investigated, notably the Ammann-Beenker tiling [60] and Fibonacci grids [61], showing superdiffusive behaviour with an exponent $\beta \geq 1/2$.

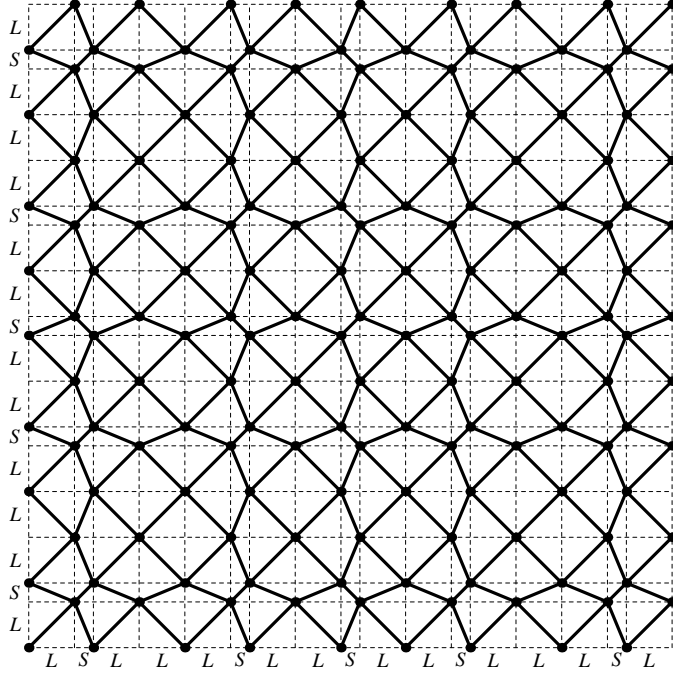


Figure 14: Labyrinth tiling constructed from a product grid (dashed) of two octonacci chains.

Here, we consider a tight-binding model on the labyrinth tiling [62], which is a planar tiling related to the octagonal tiling [63]. It is constructed from a rectangular grid based on the product of two octonacci chains (2), by connecting vertices that are separated by two steps along the grid, see Fig. 14. The two letters L and S of the substitution rule (2) are represented by a long and a short interval, respectively. Clearly, there are edges of three different lengths in the labyrinth tiling; the long edges are the diagonals of large squares formed by two L intervals, the medium edges diagonals of rectangles formed by one L and one S interval, and the short edges are the diagonals of small squares formed by two S intervals.

We define the tight-binding model on the labyrinth by the Hamiltonian (1) with on-site energies $\varepsilon_k = 0$ and non-zero hopping elements $t_{jk} = 1$, $t_{jk} = v$ and $t_{jk} = v^2$ for long, medium and short edges of the labyrinth tiling, respectively. With this choice, it can be shown that the eigenfunctions ψ_j are essentially products of two eigenfunctions of the corresponding one-dimensional tight-binding model on the octonacci chain, with hopping elements 1 and v for long and short intervals, respectively [21, 63]. The eigenenergies of the labyrinth turn out to be the products of those of the one-dimensional system. In other words, the energy spectrum and the eigenstates of the tight-binding model on the labyrinth tiling can be obtained from those of the one-dimensional octonacci chain, see [21] for details. This allows the numerical treatment of large systems, much larger than can be achieved for instance for the Ammann-Beenker tiling, because only the one-dimensional Hamiltonian needs to be diagonalised.

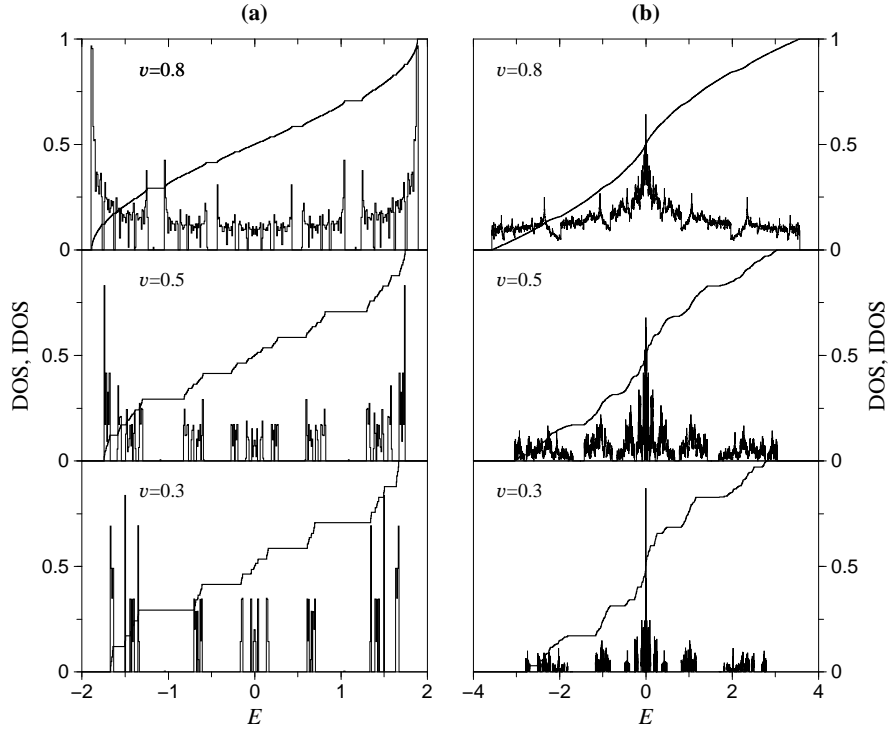


Figure 15: DOS and IDOS for the octonacci chain (left) and the labyrinth tiling (right).

In Fig. 15, the DOS and the IDOS for the octonacci chain and the labyrinth tiling are shown. It appears that for larger values of v the spectrum of the labyrinth differs qualitatively from that for small values of v , where it splits into many disjoint parts, similarly to the one-dimensional case. A more detailed investigation shows that the transition takes place around a value of $v \approx 0.6$ [21, 63].

Fig. 16 shows numerical results obtained for the temporal autocorrelation function $C(t)$. Here, we used an octonacci chain of length $N = 19\,602$, and the corresponding labyrinth thus has $N^2/2 = 19\,602^2/2 = 192\,119\,202$ vertices. A qualitative difference between the behaviour for the one-dimensional and the two-dimensional system is evident. Whereas in the one-dimensional case the exponent δ always changes with v , giving $0 < \delta < 1$ for all aperiodic systems, this does not seem to be the case for the two-dimensional system, where $\delta = 1$ for values of v between about 0.6 and 1, and $0 < \delta < 1$ only for small values of v . This is consistent with the observed qualitative change in the spectrum, as the exponent δ equals the correlation dimension D_2 of the local spectral measure associated with the initial site [56, 61].

The behaviour of the mean-square displacement is shown in Fig. 17. Here, the system size is smaller, it is 1394 for the octonacci chain shown on the left and $578^2/2 = 167\,042$ for the labyrinth tiling displayed on the right. In contrast to the autocorrelation, there is no apparent difference in the behaviour for the mean-square displacement in the two cases. In particular,

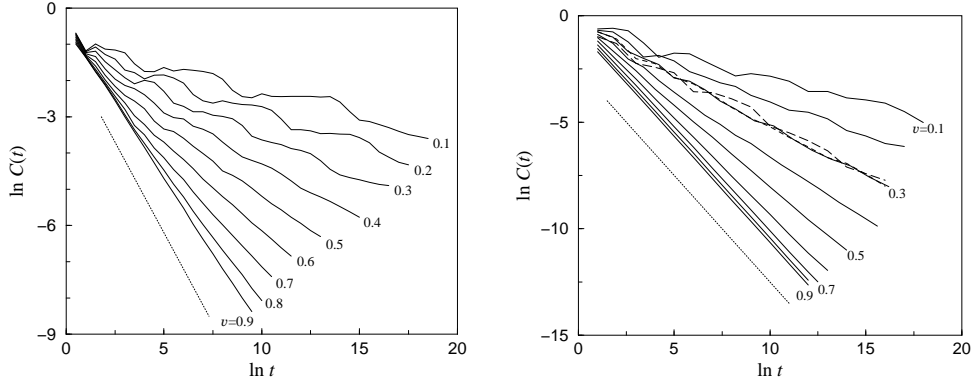


Figure 16: Autocorrelation function $C(t)$ (9) for the octonacci chain (left) and the labyrinth tiling (right). The dotted lines correspond to $C(t) \sim t^{-1}$. The dashed lines for $v = 0.3$ correspond to different choices of the initial site j_0 .

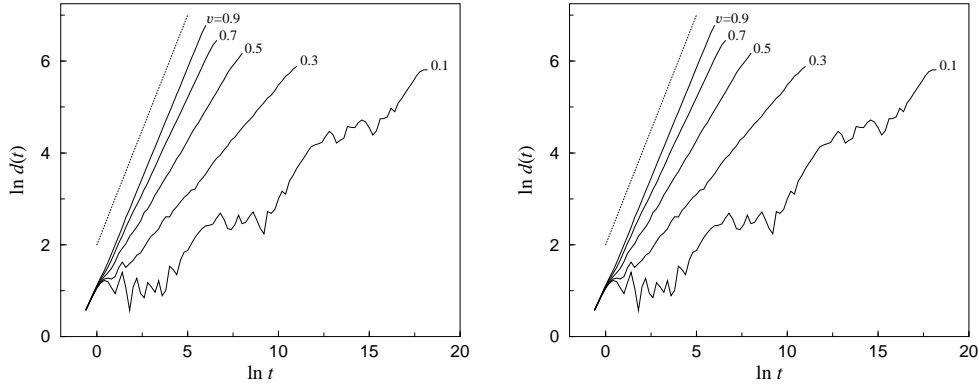


Figure 17: Mean-square displacement $d(t)$ (9) for the octonacci chain (left) and the labyrinth tiling (right). The dotted lines corresponds to ballistic motion $d(t) \sim t$.

there is no qualitative change around the value $v \approx 0.6$ where we found a transition in the spectral measure and the autocorrelation function.

Several inequalities and approximations have been derived that relate spectral properties with the exponent β characterising quantum diffusion. Quasiperiodic tight-binding Hamiltonians, due to their intricate spectral properties, provide a particularly challenging test to these results. In Fig. 18, the numerical values for β for the octonacci chain and the labyrinth tiling, for various values of the hopping parameter v , are compared with expressions involving the fractal dimensions D_q of the spectral measure and D_q^ψ of the eigenstates. In particular, the bound $\beta \geq D_2/D_2^\psi$ [57] is numerically obeyed by both the octonacci chain and the labyrinth tiling. However, the inequality is less sharp in the latter case as β is much larger than the

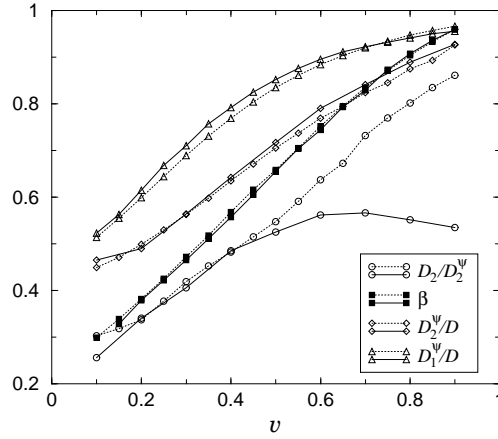


Figure 18: The exponent β compared to several quantities describing the multifractal properties of the energy spectra and wavefunctions. The lines are included to guide the eye; the dotted lines correspond to the results for the octonacci chain (dimension $D = 1$), the solid lines to the labyrinth tiling ($D = 2$).

ratio D_2/D_2^ψ , in particular for values of the parameter $v \geq 0.6$ where the energy spectrum is smooth and $D_2 \approx 1$. Another expression [64], $\beta \leq D_2^\psi/D$, where D denotes the spatial dimension, appears to be violated for parameter values of v close to one, which means close to the periodic case, though it stays reasonably close to β for all values of v . We note that the weaker condition $\beta \leq D_1^\psi/D$ appears to be always satisfied, although we presently do not know of any argument why this bound should hold. A more thorough understanding of the relations between the spectral properties and quantum diffusion is clearly desirable.

0.1.6 Interacting Electrons

All previously mentioned results, and indeed most results in the literature, are based on models of non-interacting electrons. Whereas the main effects of an interaction can often be accounted for by considering quasiparticles with effective parameters instead of bare electrons, it is not clear that electrons in quasicrystals can really be described in this way. Therefore, it is interesting to study the effect of an electron-electron interaction on the spectral properties of aperiodic Schrödinger operators. In this case, we choose the Aubry-André or Harper model mentioned above, because by changing the strength of the aperiodic modulation we can investigate extended states, critical states and localised states, and indeed study the effects of an interaction on the metal-insulator transition.

Our Hamiltonian of N interacting spinless fermions on a ring of circumference M is

$$H = - \sum_{j=1}^M c_{j+1}^\dagger c_j + c_j^\dagger c_{j+1} + V \sum_{j=1}^M n_{j+1} n_j + 2\mu \sum_{j=1}^M \cos(\alpha j + \beta) n_j, \quad (10)$$

where c_j^\dagger and c_j are fermionic creation and annihilation operators, respectively, and $n_j = c_j^\dagger c_j$ is the corresponding number operator. The hopping parameter was chosen to be one, and V denotes the strength of the interaction between the fermions. The parameter μ controls the strength of the aperiodic modulation. The aperiodicity is determined by an irrational number $\alpha/2\pi$ which we choose as $\alpha/2\pi = 1/\tau = (\sqrt{5} - 1)/2$, and β is an arbitrary shift.

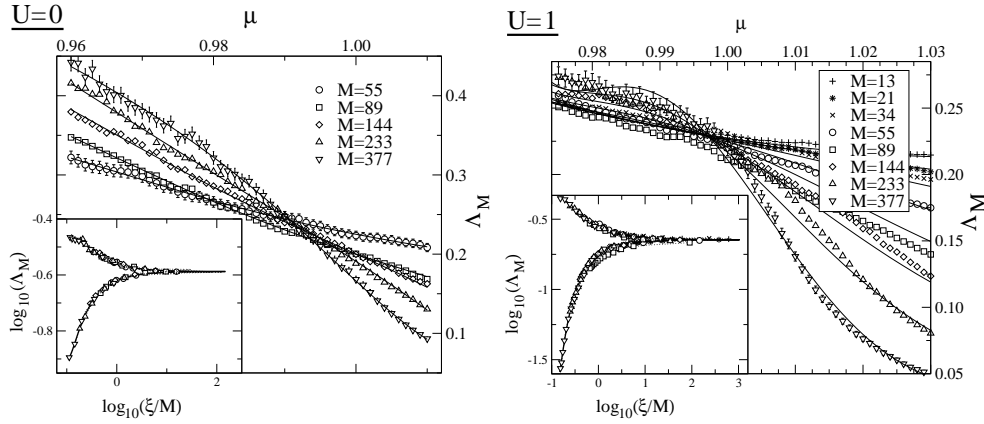


Figure 19: Dependence of the reduced localisation lengths Λ_M for systems of size M on the strength μ of the aperiodic potential, without interaction, $U = 0$ (left), and for two interacting particles with $U = 1$ (right). The insets show the scaling function in dependence on the correlation length ξ .

First, the case of very low density, meaning just two particles with opposite spin and an on-site (Hubbard) interaction U , has been investigated by means of the transfer-matrix method and finite-size scaling [32, 33, 34]. In Fig. 19, the behaviour of the reduced localisation lengths $\Lambda_M = \lambda_M/M$ [33, 34] as a function of μ is shown for the non-interacting case and the interacting case for various system sizes M . Here λ_M denotes the localisation length in the finite samples. The crossing of the interpolating lines for different M indicates the metal-insulator transition. Finite-size scaling then yields the correlation lengths for the infinite systems. For two interacting particles, the conclusion is that the metal-insulator transition remains unaffected by an on-site interaction. The observed critical potential strength is consistent with $\mu_c = 1$ also in the interacting case, and the critical exponent of the correlation lengths ξ is $\nu \approx 1$ [32, 33, 34]. For a long-range interaction the accuracy of the data is not very good, but it was observed [32] that the metal-insulator transition tends to shift to smaller values of the critical potential strength $\mu_c \approx 0.92$.

More interesting is the case of finite density $\rho = N/M$. This has been investigated by the density-matrix renormalisation-group method [35, 36] which allows us to treat systems of length up to $M \approx 100 - 200$, whereas direct diagonalisation techniques are limited to very small system sizes. A convenient observable to investigate the metal-insulator transition, in this case, is the phase sensitivity

$$M \Delta E = (-1)^N M [E(0) - E(\pi)] \quad (11)$$

of the ground state [35, 36], where $E(\varphi)$ denotes the ground-state energy of the system with a twist $c_{M+1} = \exp(i\varphi)c_1$ at the boundary. This quantity is independent of the system size for extended wave functions and decreases exponentially with system size if the wave function is localised. In this case, it turns out that the behaviour of the system depends on the particle density ρ . If ρ is incommensurate with the parameter $\alpha/2\pi$, the system behaves very much

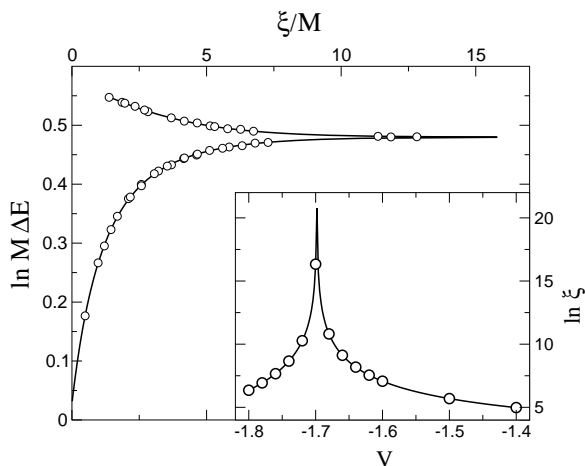


Figure 20: Scaled data of the phase sensitivity $M \Delta E$ (11) for the model of Eq. (10) with parameter $\alpha/2\pi = \tau^{-1}$, particle density $\varrho_3 = \tau^{-3}$, potential $\mu = 0.4$, interaction parameters $V \in [-1.8, -1.4]$ and various system sizes M . The inset shows the scaling parameter ξ .

like the one with two interacting particles. For attractive or repulsive interaction, one finds a critical potential strength $\mu_c \approx 1$ and a critical exponent $\nu \approx 1$ for the phase sensitivity $M \Delta E \sim (\mu_c - \mu)^\nu$ near criticality.

For particle densities ϱ that are commensurate with $\alpha/2\pi = \tau^{-1}$, for instance for $\varrho_n = \tau^{-n}$, a different behaviour is observed. This may be understood most easily for $\varrho_1 = \tau^{-1}$ where the resonance condition $\alpha = 2k_F$ holds for the Fermi wave vector $k_F = \pi\varrho$. In this case, one may expect to find a Peierls-like transition [65], and this is indeed observed [35, 36]. The phase diagram for fixed commensurate density ϱ appears to be dominated by localised states, at a given potential strength $\mu > \mu_{\min}$, with a regime of extended states for small values of μ in a certain range of interaction strengths V . For repulsive and weakly attractive interactions, the ground state for $\mu > \mu_{\min}$ is localised. For strongly attractive interactions, the system shows Peierls-like behaviour, meaning that there is a transition from the insulating to a metallic phase around $V \approx -\sqrt{2}$ [35, 36]. As an example, the scaling function obtained for the density $\varrho_3 = \tau^{-3} \approx 0.236$ and potential $\mu = 0.4$ is shown in Fig. 20.

In summary, for the incommensurate case the interaction does not seem to affect the metal-insulator transition in this system. For the commensurate case, the behaviour is dominated by the resonance which leads to Peierls-type behaviour.

0.1.7 Concluding Remarks

Though there has been considerable progress over the last two decades, our understanding of the physical properties of quasicrystals is still far from complete, as is the knowledge about their structure [2, 4] and the physical growth mechanism [66]. Concerning their electronic properties, there exist several approaches that can, at least, qualitatively account for the peculiar features of quasicrystals.

Here, we discussed spectral properties of discrete aperiodic Schrödinger operators based on numerical and analytic investigations. Whereas one-dimensional models are reasonably well understood, our present knowledge of the two-dimensional systems rests largely on numerical investigations of a few examples, notably the Penrose and Ammann-Beenker tilings.

For these models, numerical results establish multifractal behaviour of generic eigenstates, which is corroborated by the analytical construction of such states for the Penrose tiling. A statistical investigation of the energy spectrum shows, somewhat surprisingly, that the level-spacing distribution of such models appears to be extremely well described by universal random matrix distributions, and that there is no “critical” statistics as one might have guessed from the multifractal character of the eigenstates. Furthermore, we discussed quantum diffusion by numerically investigating a tight-binding model on a peculiar tiling, the labyrinth, which has the property that all eigenenergies and eigenstates can be obtained as products of those of a one-dimensional tight-binding model on the octonacci chain. Our results corroborate that there are strong relations between fractal properties of energy spectra and wavefunctions on the one hand and the exponents describing the quantum diffusion on the other hand. However, it appears to be difficult to find relations that give quantitative agreement for one- and two-dimensional aperiodic systems. Here, a deeper understanding of the underlying physics is desirable. Higher-dimensional systems constructed as products of one-dimensional systems, such as the labyrinth tiling, may provide useful toy examples for further investigations which can, at least, be treated numerically in an efficient way. Finally, the role of an electron-electron interaction on the metal-insulator transition in a one-dimensional aperiodic system was investigated. The results show that resonance-type phenomena are important, giving rise to a different behaviour for particle densities which are commensurate and incommensurate with the modulation. In the incommensurate case, only minor effects can be seen, whereas Peierls-like transitions are observed for the commensurate case.

Not much is known for three-dimensional systems, though it appears plausible, and consistent with our numerical results, that there is a general tendency that eigenstates become less localised with increasing spatial dimension. However, many questions remain unanswered, and it is not even decided whether extended states exist in models such as the tight-binding model on the Ammann-Kramer-Neri tiling considered here. Other interesting questions concern transport in quasiperiodic systems in the presence of magnetic fields, see for instance [67] for a glimpse at the complexity of such systems.

Acknowledgement

This work was supported by Deutsche Forschungsgemeinschaft (Schr 231/16). UG would like to thank the Erwin Schrödinger International Institute for Mathematical Physics in Vienna for support during a stay in December 2002 where this work was completed.

Bibliography

- [1] U. Grimm and M. Scheffer, Incommensurate Crystals and Quasicrystals. In: R. A. Meyers, editor, *Encyclopedia of Physical Science and Technology*. 3rd ed., vol. 7, Academic Press, San Diego (2001) 731–750.
- [2] Z. M. Stadnik, editor, *Physical Properties of Quasicrystals* Springer, Berlin (1999).
- [3] M. Baake and R. V. Moody, editors, *Directions in Mathematical Quasicrystals* American Mathematical Society, Providence, RI (2000).

- [4] J.-B. Suck, M. Schreiber and P. Häussler, editors, *Quasicrystals — An Introduction to Structure, Physical Properties, and Applications* Springer, Berlin (2002).
- [5] M. Baake and U. Grimm, Further reading: Literature on quasicrystals. In: [4] 539–544.
- [6] G. Kasner, H. Schwabe and H. Böttger, Conductance of quasiperiodic model systems, this volume.
- [7] S. Klassert, D. Lenz and P. Stollmann, Delone dynamical systems: Ergodic features and applications, this volume.
- [8] H. Solbrig and C. Landauro, Electronic transport parameters and spectral fine structure: From approximants to quasicrystals, this volume.
- [9] P. Häussler, R. Haberkern, J. Barzola-Quijia, C. Madel, K. Khedri and M. Lang, Quasicrystals — models for matter from the disordered to the ordered state, this volume.
- [10] J. Kroha, D. Walther and R. von Baltz, Interrelations between atomic and electronic structures in quasicrystals, this volume.
- [11] B. Simon, Almost periodic Schrödinger operators: A review, *Adv. Appl. Math.* **3** (1982) 463–490.
- [12] D. Damanik, Gordon-Type arguments in the spectral theory of one-dimensional quasicrystals. In: [3] 277–305; math-ph/9912005.
- [13] P. W. Anderson, Absence of diffusion in certain random lattices, *Phys. Rev.* **109** (1958) 1492–1505.
- [14] M. Schreiber, Fractal character of eigenstates in weakly disordered three-dimensional systems, *Phys. Rev. B* **31** (1985) 6146–6149.
- [15] M. Schreiber and H. Grussbach, Multifractal wave functions at the Anderson transition, *Phys. Rev. Lett.* **67** (1991) 607–610.
- [16] H. Grussbach and M. Schreiber, Multifractality of wave functions and wave packets at the metal-insulator transition in the Anderson model of localization, *Physica A* **191** (1992) 394–400.
- [17] H. Grussbach and M. Schreiber, Determination of the mobility edge in the Anderson model of localization in three dimensions by multifractal analysis, *Phys. Rev. B* **51** (1995) 663–666.
- [18] E. Hofstetter and M. Schreiber, Finite-size scaling and critical exponents. A new approach and its applications to Anderson localization, *Europhys. Lett.* **27** (1993) 933–939.
- [19] E. Hofstetter and M. Schreiber, Statistical properties of the eigenvalue spectrum of the three-dimensional Anderson Hamiltonian, *Phys. Rev. B* **48** (1993) 16979–16985.
- [20] E. Hofstetter and M. Schreiber, Relation between energy-level statistics and phase transitions and its applications to the Anderson model, *Phys. Rev. B* **49** (1994) 14726–14729; cond-mat/9402093.
- [21] H. Yuan, U. Grimm, P. Repetowicz and M. Schreiber, Energy spectra, wavefunctions and quantum diffusion for quasiperiodic systems, *Phys. Rev. B* **62** (2000) 15569–15578; cond-mat/9912176.
- [22] J. Bellissard, A. Bovier and J. M. Ghez, Gap labelling theorems for one-dimensional discrete Schrödinger operators, *Rev. Math. Phys.* **4** (1992) 1–37.

- [23] M. Baake, U. Grimm and D. Joseph, Trace maps, invariants, and some of their applications, *Int. J. Mod. Phys. B* **7** (1993) 1527–1550; math-ph/9904025.
- [24] X. Wang, U. Grimm and M. Schreiber, Trace and antitrace maps for aperiodic sequences: Extensions and applications, *Phys. Rev. B* **62** (2000) 14020–14031; cond-mat/0005463.
- [25] R. Ammann, B. Grünbaum and G. C. Shephard, Aperiodic tiles, *Discrete Comput. Geom.* **8** (1992) 1–25.
- [26] M. Baake, U. Grimm and R. V. Moody, Die verborgene Ordnung der Quasikristalle, *Spektrum der Wissenschaft* (February 2002) 64–74.
- [27] M. Baake, U. Grimm and R. V. Moody, What is aperiodic order? math.HO/0203252.
- [28] U. Grimm and M. Schreiber, Aperiodic tilings on the computer, in [4] 49–66; cond-mat/9903010.
- [29] P. Kramer and R. Neri, On periodic and non-periodic space fillings of E^m obtained by projection, *Acta Cryst. A* **40** (1984) 580–587; *Acta Cryst. A* **41** (1985) 691 (Erratum).
- [30] T. Rieth and M. Schreiber, Identification of spatially confined states in two-dimensional quasiperiodic lattices, *Phys. Rev. B* **51** (1995) 15827–15832.
- [31] S. Aubry and G. André, Analyticity breaking and Anderson localization in incommensurate lattices, *Ann. Israel Phys. Soc.* **3** (1980) 133–164.
- [32] A. Eilmes, U. Grimm, R. A. Römer and M. Schreiber, Two interacting particles at the metal-insulator transition, *Eur. Phys. J. B* **8** (1999) 547–554; cond-mat/9808192.
- [33] A. Eilmes, R. A. Römer and M. Schreiber, Localization properties of two interacting particles in a quasi-periodic potential with a metal-insulator transition, *Eur. Phys. J. B* **23** (2001) 229–234; cond-mat/0106603.
- [34] A. Eilmes, R. A. Römer and M. Schreiber, Localization properties of two interacting particles in a quasiperiodic potential with a metal-insulator transition, *Proceedings of ICPS26* (to appear).
- [35] C. Schuster, R. A. Römer and M. Schreiber, Interacting particles at a metal-insulator transition, *Phys. Rev. B* **65** (2002) 115114, 1–7; cond-mat/0102251.
- [36] C. Schuster, R. A. Römer and M. Schreiber, Commensurate and incommensurate transitions for interacting particles, *J. Phys. Soc. Japan* (to appear).
- [37] T. Rieth and M. Schreiber, Numerical investigation of electronic wave functions in quasiperiodic lattices, *J. Phys.: Condens. Matter* **10** (1998) 783–800.
- [38] T. Rieth, U. Grimm and M. Schreiber, Localization of electronic wave functions on quasiperiodic lattices. In: S. Takeuchi and T. Fujiwara, editors, *Proceedings of the 6th International Conference on Quasicrystals*. World Scientific, Singapore (1998) 639–642; cond-mat/9809117.
- [39] T. Rieth and M. Schreiber, The Anderson transition in three-dimensional quasiperiodic lattices: Finite-size scaling and critical exponent, *Z. Phys. B* **104** (1997) 99–102.
- [40] B. I. Shklovskii, B. Shapiro, B. R. Sears, P. Lambrianides and H. B. Shore, Statistics of spectra of disordered systems near the metal-insulator transition, *Phys. Rev. B* **47** (1993) 11487–11490.
- [41] M. L. Mehta, *Random Matrices*. 2nd ed., Academic Press, Boston (1990).
- [42] I. K. Zharekeshev and B. Kramer, Asymptotics of universal probability of neighboring level spacings at the Anderson transition, *Phys. Rev. Lett.* **79** (1997) 717–720.

- [43] V. G. Benza and C. Sire, Band spectrum of the octagonal quasicrystal: Finite measure, gaps, and chaos, *Phys. Rev. B* **44** (1991) 10343–10345.
- [44] F. Piéchon and A. Jagannathan, Energy-level statistics of electrons in a two-dimensional quasicrystal, *Phys. Rev. B* **51** (1995) 179–184.
- [45] J.-X. Zhong, U. Grimm, R. A. Römer and M. Schreiber, Level-spacing distributions of planar quasiperiodic tight-binding models, *Phys. Rev. Lett.* **80** (1998) 3996–3999; *cond-mat/9710006*.
- [46] M. Schreiber, U. Grimm, R. A. Römer and J.-X. Zhong, Application of random matrix theory to quasiperiodic systems, *Physica A* **266** (1999) 477–480; *cond-mat/9809370*.
- [47] M. Schreiber, U. Grimm, R. A. Römer and J.-X. Zhong, Energy levels of quasiperiodic Hamiltonians, spectral unfolding, and random matrix theory, *Comp. Phys. Commun.* **121–122** (1999) 499–501; *cond-mat/9811359*.
- [48] U. Grimm, R. A. Römer, M. Schreiber and J.-X. Zhong, Universal level-spacing statistics in quasiperiodic tight-binding models, *Mat. Sci. Eng. A* **294–296** (2000) 564–567; *cond-mat/9908063*.
- [49] J. X. Zhong and T. Geisel, Level fluctuations in quantum systems with multifractal eigenstates, *Phys. Rev. E* **59** (1999) 4071–4074.
- [50] U. Grimm, R. A. Römer and G. Schliecker, Electronic states in topologically disordered systems, *Ann. Phys. (Leipzig)* **7** (1998) 389–393; *cond-mat/9811360*.
- [51] A. Jagannathan, Self-similarity under inflation and level statistics: A study in two dimensions, *Phys. Rev. B* **61** (2000) R834–R837; *cond-mat/9909104*.
- [52] B. Sutherland, Self-similar ground-state wave function for electrons on a two-dimensional Penrose lattice, *Phys. Rev. B* **34** (1986) 3904–3909.
- [53] T. Tokihiro, T. Fujiwara M. and Arai, Exact eigenstates on a two-dimensional Penrose lattice and their fractal dimensions, *Phys. Rev. B* **38** (1988) 5981–5987.
- [54] P. Repetowicz, U. Grimm and M. Schreiber, Exact eigenstates of tight-binding Hamiltonians on the Penrose tiling, *Phys. Rev. B* **58** (1998) 13482–13490; *cond-mat/9805321*.
- [55] P. Repetowicz, U. Grimm and M. Schreiber, High-temperature expansion for Ising models on quasiperiodic tilings, *J. Phys. A: Math. Gen.* **32** (1999) 4397–4418; *cond-mat/9901001*.
- [56] R. Ketzmerick R., G. Petschel and T. Geisel, Slow decay of temporal correlations in quantum systems with Cantor spectra, *Phys. Rev. Lett.* **69** (1992) 695–698.
- [57] R. Ketzmerick, K. Kruse, S. Kraut and T. Geisel, What determines the spreading of a wave packet? *Phys. Rev. Lett.* **79** (1997) 1959–1962; *cond-mat/9611006*.
- [58] I. Guarneri, Spectral properties of quantum diffusion on discrete lattices, *Europhys. Lett.* **10** (1989) 95–100.
- [59] I. Guarneri, On an estimate concerning quantum diffusion in the presence of a fractal spectrum, *Europhys. Lett.* **21** (1993) 729–733.
- [60] B. Passaro, C. Sire and V. G. Benza, Anomalous diffusion and conductivity in octagonal tiling models, *Phys. Rev. B* **46** (1992) 13751–13755.
- [61] J. X. Zhong and R. Mosseri, Quantum dynamics in quasiperiodic systems, *J. Phys.: Condens. Matter* **7** (1995) 8383–8404.

- [62] C. Sire, R. Mosseri and J.-F. Sadoc, Geometric study of a 2D tiling related to the octagonal quasiperiodic tiling, *J. Phys. France* **50** (1989) 3463–3476.
- [63] C. Sire, Electronic spectrum of a 2D quasi-crystal related to the octagonal quasiperiodic tiling, *Europhys. Lett.* **10** (1989) 483–488.
- [64] J. X. Zhong, Z. Y. Zhang, M. Schreiber, E. W. Plummer and Q. Niu, Dynamical scaling properties of electrons in quantum systems with multifractal eigenstates, *cond-mat/0011118*.
- [65] R. E. Peierls, *Quantum Theory of Solids*. Oxford University Press, Oxford (1955).
- [66] U. Grimm and D. Joseph, Modelling quasicrystal growth, in [4] 199–218; *cond-mat/9903074*.
- [67] U. Grimm, F. Gagel and M. Schreiber, Magnetotransport in quasilattices. In: S. Takeuchi and T. Fujiwara, editors, *Proceedings of the 6th International Conference on Quasicrystals*. World Scientific, Singapore (1998) 188–191; *cond-mat/9809114*.